Adaptive Filtering to Enhance Noise Immunity of Impedance and Admittance Spectroscopy: Comparison with Fourier Transformation

Daniil D. Stupin,[1,*] Sergei V. Koniakhin,[1] Nikolay A. Verlov,[1,2] and Michael V. Dubina[1,3]

[1]*St. Petersburg Academic University, Khlopina 8/3, 194021 St. Petersburg, Russia*

[2]*Petersburg Nuclear Physics Institute NRC "Kurchatov Institute," Gatchina, St. Petersburg 188300, Russia*

[3]*Peter the Great St. Petersburg Polytechnic University, Polytechnicheskaya str. 29, 195251 St. Petersburg, Russia*

(Received 24 January 2017; revised manuscript received 31 January 2017; published 30 May 2017)

The time-domain technique for impedance spectroscopy consists of computing the excitation voltage and current response Fourier images by fast or discrete Fourier transformation and calculating their relation. Here we propose an alternative method for excitation voltage and current response processing for deriving a system impedance spectrum based on a fast and flexible adaptive filtering method. We show the equivalence between the problem of adaptive filter learning and deriving the system impedance spectrum. To be specific, we express the impedance via the adaptive filter weight coefficients. The noise-canceling property of adaptive filtering is also justified. Using the RLC circuit as a model system, we experimentally show that adaptive filtering yields correct admittance spectra and elements ratings in the high-noise conditions when the Fourier-transform technique fails. Providing the additional sensitivity of impedance spectroscopy, adaptive filtering can be applied to otherwise impossible-to-interpret time-domain impedance data. The advantages of adaptive filtering are justified with practical living-cell impedance measurements.

DOI: 10.1103/PhysRevApplied.7.054024

I. INTRODUCTION

Electrical immittance (impedance and admittance) spectroscopy [1,2] (EIS) is a powerful tool for electronic device diagnostics [3–5], materials characterization [6–11], electrochemistry [12–14], alternative energy sources investigation [15–18], and experiments in biophysics [19–24]. The research of dynamic systems has become a hot topic of impedance spectroscopy in recent years. The excitation voltage (EV) with broad-frequency spectrum such as like rectangular pulses, peaks, various types of noise, linear sweep, or superposition of sine waves is commonly used for time-resolved immittance spectroscopy. Employing such excitation signals allows one to scan the sample in the wide-frequency range, which gives a significant advantage in performance and time resolution with respect to single-sine methods. To obtain the immittance spectrum (IS) from the collected data, the fast and discrete Fourier transform (FFT DFT) [25,26] of the EV and current response is used [27–29]. Further which, the investigated system parameters are estimated by fitting the obtained IS with the complex nonlinear least squares (CNLS) method [30].

Obviously, the nature of dynamic and nonreversible systems does not allow experiment replication for data accumulation for the following statistical noise canceling (averaging signal technique). To study them, technological improvements such as shielding, increasing the EV, varying the geometry of electrodes, or low-noise electronics usage are required for increasing the signal-to-noise ratio (SNR). If the sample produces its own noise or when the above-mentioned methods are impractical, the obtained raw IS is distorted by noises and interferences, which complexifies the data analysis. The FFT does not provide the noise-canceling option by itself, and, thus, the results of the CNLS method can be unreliable. To the best of our knowledge, only the weighting method is currently used in this case for the CNLS fit [1,2,31]. If this approach does not succeed, the IS data cannot be interpreted, and no information about the studied system can be gained.

The progressive signal processing methods (Kalman filtering [32,33], adaptive filtering [34], and other [26]) allows the extraction more information from high-noise data. The possibility of the adaptive filtering (AF) application for IS processing has been previously noticed [15]. This approach can provide the solution to the problem mentioned above due to the noise-canceling property of AF in the identification mode (learning) [34]. Combination of AF with the usage of the broad-frequency-spectrum excitation signal, like in the standard FFT method, provides decreasing the instrument influence on the sample and increasing the time and frequency resolution [27–29,35,36] as high as it is principally possible. In addition, AF requires relatively small computation power and available memory, which is important for online applications and creating

*Stu87@ya.ru, Stupin@spbau.ru

portable devices. The information about the IS is stored in weight coefficients (WC), which results in decreasing the memory requirement for IS data storage and increasing the IS data transfer speed. Finally, after the adaptive filter learning phase, AF opens the direct way to create a digital model resembling the behavior of the investigated system, which is useful for its further simulation.

Despite the successful application of the AF algorithm for the IS treatment in Ref. [15], no theoretical background has been given for this approach, and no comparison with other methods has been done. The present study is devoted to the elucidation of these aspects.

In this paper, we develop the theory of AF application for EIS. We analyze the relationship between the adaptive filter weight coefficients and the IS, derive the apparatus and weight functions of the AF method, and theoretically justify its noise immunity. We experimentally show that the AF method is more accurate than the FFT method, especially for high-noise raw data.

The paper is organized as follows. In Sec. II A, we introduce the AF model employed, and in Sec. II B, we provide the derivation of the system immittance on the basis of AF parameters, namely, weight coefficients. In Sec. III, we describe the experimental setup for measuring the immittance. In Sec. IV, on the basis of the obtained experimental data, we justify the noise immunity property of AF with respect to the FFT. In Sec. V, we illustrate the power of AF by demonstrating its application in EIS-based *in vitro* cell biosensing.

II. THEORY

A. Model

For processing the IS on the basis of the AF method, the investigated sample can be considered as a linear "black box" (Fig. 1). The experimentally measured quantities are the excitation voltage V_k being the input signal and current response J_k being the output signal, or in the terms of AF, the desired signal. Index k here is the time counter. The additive current noise ε_k can also arise during measurements due to the sample's own noise, external noise, or interferences. We now introduce J_k^a as predictions of the adaptive filter:

$$J_k^a = \sum_{j=1}^{\ell_d} d_j J_{k-j}^a + \sum_{j=0}^{\ell_n} n_j V_{k-j}, \tag{1}$$

where d_j and n_j are WC, and the maximum value between ℓ_d and ℓ_n is the filtering order. So, Eq. (1) describes the causal (without loss of generality) discrete filter with infinite impulse response (IIR) [26]. By adjusting the WC, the following functional is minimized over all measurement result,

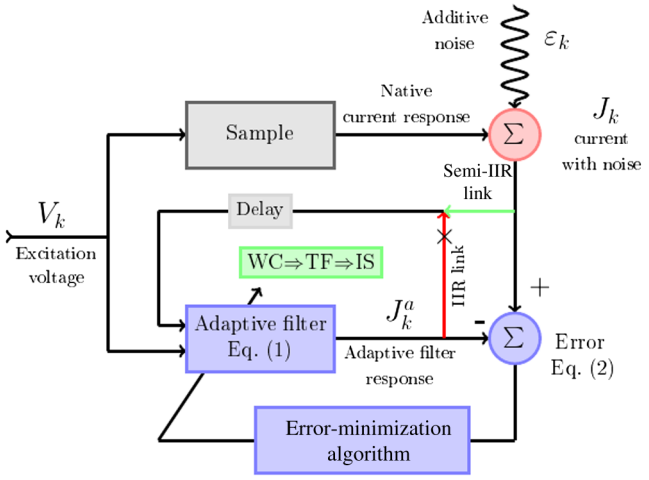

FIG. 1. Processing the IS on the basis of the AF method. The classical AF identification system with infinite impulse response (IIR) corresponds to the enabled IIR link (red) and disabled semi-IIR link (green). If the IIR link is disabled and if the semi-IIR link is enabled this scheme describes the semi-IIR model. If both links are disabled, the scheme describes the model with finite impulse response (FIR). The acronyms used in the figure are weight coefficients (WC), transfer function (TF), and immittance spectrum (IS).

$$\sum_{k=\max(\ell_n,\ell_d)}^{L} |J_k^a - J_k|^2 = \min, \tag{2}$$

where $L+1$ is the total number of collected samples. The transfer function of Eq. (1) with the adjusted WC can be considered as an approximation of the sample admittance [15], as we show in Sec. II B.

It is well known that the IIR filters are more flexible than the FIR filters. However, searching for the WC values of the IIR filters requires sufficient computation power, and a principal problem of the functional (2) local minimums exists [34]. To increase flexibility on the one hand and to simplify the WC search on another hand, this paper introduces the semi-IIR filter model. Namely, we replace in the right-hand part of Eq. (1) J_k with J_k^a before substituting it to Eq. (2). Thus, the functional to be minimized takes the form

$$\sum_{k=\max(\ell_n,\ell_d)}^{L} \left| J_k - \sum_{j=1}^{\ell_d} d_j J_{k-j} - \sum_{j=0}^{\ell_n} n_j V_{k-j} \right|^2 = \min. \tag{3}$$

Equation (3) describes the operating principle of AF with V_k for the input signal and J_k for the desired response and for the AF prediction simultaneously. Note that the beginning of the summation from $j=1$ for d_j in Eq. (3) prevents the trivial solution $d_0 = 1$, $d_j = 0$ when $j > 0$ and $n_j = 0$. The developed theory is also applicable to the FIR filters [15] characterized by fixing $d_j = 0$ and $\ell_d = 0$, and to the noncausal FIR and the noncausal semi-IIR filter models.

B. The relation between the time and frequency domain

We now discuss the possibility of IS estimation with Eq. (3). To simplify our analysis, we neglect the measurement noise ε_k. If the sample rate f_0 is high enough, one can change the summation by k in Eq. (3) with integration over the data-collecting interval $[-T/2, T/2]$. On the basis of Parseval's identity, one can write the following:

$$\begin{aligned}&\int_{-T/2}^{T/2}\left|J(t)-\sum_{j=1}^{\ell_d} d_j J(t-j\Delta t)-\sum_{j=0}^{\ell_n} n_j V(t-j\Delta t)\right|^2 dt\\&=\int_{-\infty}^{+\infty}\left|J(t)-\sum_{j=1}^{\ell_d} d_j J(t-j\Delta t)-\sum_{j=0}^{\ell_n} n_j V(t-j\Delta t)\right|^2 \Pi dt\\&=2\pi\int_{-\infty}^{+\infty}\left|\left(1-\sum_{j=1}^{\ell_d} d_j\varphi_j\right)J(f)-V(f)\sum_{j=0}^{\ell_n} n_j\varphi_j\right|^2 * K df,\end{aligned} \tag{4}$$

where Π is rectangular function with $[-T/2, T/2]$ width, with the Fourier image given by the sinc function

$$K=\frac{\sin(\pi f T)}{\pi f}, \tag{5}$$

$\varphi_j(f)=\exp[2\pi i j(f/f_0)]$ is the Fourier image of the impulse delayed by $\Delta t = 1/f_0$, f is the frequency, the asterisk * denotes convolution, and $V(f)$ and $J(f)$ are Fourier images of the voltage and current, respectively. Now we use Ohm's law $J(f)=YV(f)$, where Y is the admittance of the system at frequency f, and we omit the 2π multiplier. Thus, from Eq. (4), one can write for the functional to be minimized:

$$\begin{aligned}\int_{-\infty}^{+\infty}\Bigg[&\left|\left(1-\sum_{j=1}^{\ell_d} d_j\varphi_j\right)Y-\sum_{j=0}^{\ell_n} n_j\varphi_j\right|^2\\&\times|V(f)|^2\Bigg] * K df=\min.\end{aligned} \tag{6}$$

Let us analyze Eq. (6). It is simple to see that K plays the role of the apparatus function, which defines the frequency resolution of the method Δf. The latter can be calculated as the distance between the first positive and the first negative roots of K, which can be estimated as

$$\Delta f=\frac{1}{T}. \tag{7}$$

If the data-collection time T is long enough, K can be replaced with the δ function, which allows us to omit the convolution in Eq. (6). Henceforth, we take convolution into account only as the restriction on the frequency resolution.

In these assumptions, the squared magnitude of the EV image $|V(f)|^2$ is the weight function. Variation of its shape gives the possibility to control the influence of the selected frequency ranges on the IS processing.

According to Kotelnikov's theorem, the condition $f_B \le f_0/2$ must be met, where f_B is the highest harmonic the exciting signal generator can produce. As a result, we obtain the following hierarchy of the characteristic setup frequencies:

$$\Delta f \ll f_B \le f_0/2. \tag{8}$$

The most illustrative and practical case is the case of the excitation voltage with $|V(f)|=\text{const}$ in the frequency band $f \le f_B$. The excitation voltage types satisfying this condition are the white-noise, linear-sweep, and δ-function signals. Thus, Eq. (6) takes the form

$$\int_{-f_B}^{+f_B}\left|\left(1-\sum_{j=1}^{\ell_d} d_j\varphi_j\right)Y-\sum_{j=0}^{\ell_n} n_j\varphi_j\right|^2 df=\min. \tag{9}$$

The integrand for the case of IIR filter usage can be obtained by dividing the integrand in Eq. (9) by the squared absolute value of the expression in parentheses.

Equation (9) is, in fact, the Levy approximation [37] for the admittance Y with φ_j being the basis functions, and one can write the following estimation of the admittance:

$$Y\approx\left(\sum_{j=0}^{\ell_n} n_j\varphi_j\right)\Big/\left(1-\sum_{j=1}^{\ell_d} d_j\varphi_j\right). \tag{10}$$

One sees that the admittance Y is directly derived from WC obtained by minimization of the functional in Eq. (3) with experimentally measured sequences of V_k and J_k substituted. The AF method does not rely on the FFT, which gives the advantage of memory economy. Since the admittance estimation (10) is derived from Eq. (9) heuristically, there is no obvious preference to use admittance Y or impedance $Z=1/Y$ for the IS analysis.

In the special case of the FIR filter [the denominator in Eq. (10) is equal to 1] together with the additional condition $f_B = f_0/2$, the WC n_j are straightforwardly the Fourier coefficients of admittance. This means that any admittance, which can be expanded into Fourier series in the $\pm f_b$ interval (including ideal circuits and the Warburg impedance), can be estimated by AF with any accuracy. In practice, the most actual case is $f_0 \gg f_B$. Thus, for low enough AF order (ℓ_d, $\ell_n \ll f_0/f_B$), the $\varphi_j(f)$ arguments $2\pi i j(f/f_0)$ are much less than 1. This means that the exponential functions $\varphi_j(f)$ can be expanded into the Taylor series, and Eq. (10) becomes a rational function (standard Levy approximation) with the coefficients being a linear combination of n_j and d_j.

Typically, the admittances of real systems are given by rational functions or expandable into the Taylor and Fourier series. However, the straight algebraic relation between the parameters of the studied system (the ratings of resistors, capacitors, and inductors the system is formed of) and the WC is complicated. Therefore, we suggest using Eq. (10) to obtain the frequency dependence of immittance. Because of the noise-canceling property of AF, the yield of Eq. (10) can be considered as a noise-free approximation of the real IS. Then, the system parameters can be derived by applying the standard methods to the obtained IS: algebraic method (AM) [38], geometric methods [39], or CNLS [30].

The procedure of the functional (3) minimization and the noise-canceling property of AF are discussed in Appendixes A and B, respectively.

III. EXPERIMENT

The linear-sweep-shape signal with 20-mV peak-to-peak amplitude generated by the signal generator AKIP-3413-3 (AKIP, Russia, two channels) is used as excitation voltage. The frequency range is from 10 Hz to 40 kHz, and the sweep time is 500 ms.

For the J_k measurements, an ammeter (current-to-voltage converter) based on the operational amplifier AD8606 (Analog Devices, USA) is assembled. It should be noticed that the AD8606 has unity-gain frequency $f_s = 10$ MHz, and virtual inductance L_V of about several millihenrys can arise due to the used backfeed resistor $R_0 = 100$ kΩ. The corresponding equation reads as $L_V = R_0/(2\pi f_s)$.

The L-Card E20-10 analog-to-digital converter (ADC) (LCard, Russia, 10 MHz band, 12 bits, four channels) is used in this study to record the excitation voltage V_k and current response J_k from the ammeter output. The data collection time T is 500 ms and the sampling rate $f_0 = 500$ kHz, which yields 250 000 collected samples. One sees that the experimental setup parameters obey the required frequencies' hierarchy Eq. (8) and the constant EV spectrum assumption (see Appendix C). The setup scheme is shown in Fig. 2.

The serial RLC circuit is used as a sample. The DT9205A multimeter (Resanta, Russia) yields the reference values of

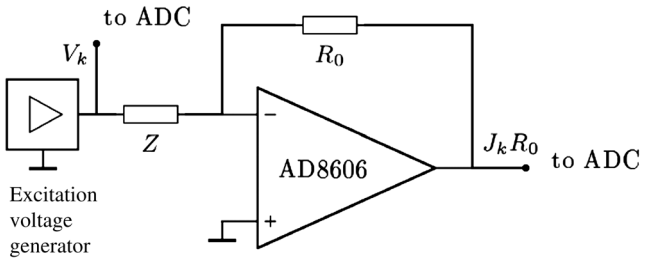

FIG. 2. Setup for IS measurement using the time-domain technique. The operational amplifier is connected into the current-to-voltage converter circuit. Here, Z is the unknown sample impedance, and R_0 is the feedback resistor.

the circuit elements $C_m = 10$ nF, $R_m = 250$ Ω, and the inductance factory rating is 15 mH. The measurements are conducted with various SNRs. To decrease the SNR, the interference source (transformer connected to the generating white-noise-shaped signal second channel of the AKIP-3413-3) is placed near the RLC circuit. This is a simulation of the usual experimental practice: any electronic device (microscope, computer, display, motors, transformers, and power electronics) located in close proximity to the sample produces interference. This method resembles, e.g., an electrical biological cell-substrate impedance-sensing device [20] or single-cell EIS [40] with microscope control (see Sec. V). The SNR values are calculated as the relation between the noise-free J_k root-mean-squares (rms) (EV output on, noise generator off) and the noise rms (EV output off, noise generator output on).

To obtain lower values of the SNR, a simulation with digital artificial noise is conducted. The values ε_k are generated by the MATLABs' random routine randn and added to the current response J_k obtained with the highest experimental SNR (30 dB). To achieve the statistics, the data are collected over four experiments for each SNR for experimental and artificial digital noise.

To implement the AF-based derivation of the IS, the above-introduced semi-IIR model with $\ell_d = 49$ and $\ell_n = 101$ is used. To obtain the IS with the FFT, the Fourier images of V_k and J_k are calculated in MATLAB.

For further IS CNLS parameters fitting the MATLAB code NELM based on the Nelder-Mead simplex algorithm [41] is written. The latter may be obtained from the authors. The freeware LEVM program [31] by Ross Macdonald and the ORIGIN package are not suitable for this purpose due to the impossibility of processing a large input data set and supporting CUDA technology to decrease the runtime. The initial values of R, L, and C for the CNLS fit are 256 Ω, 19.4 mH, and 9.207 nF, respectively.

IV. RESULTS AND DISCUSSION

The dependence of the circuit elements' ratings obtained by CNLS fit on the SNR for the IS obtained by the AF and FFT methods are presented in Fig. 4. In Fig. 3, the spectra and the corresponding CNLS fits for the 30- and 3-dB SNRs are shown. The corresponding CNLS fit results are listed in Table I. One sees that the AF method is robust with respect to the decreasing SNR.

At low SNR, the spectra obtained by the FFT are drastically distorted, which leads to incorrect estimation of R, L, and C in the CNLS fit. The FFT and CNLS fits fail at low SNR even in the case where the correct ratings obtained at high SNR are used as the initial fitting parameters. The discrepancy in the capacitance value is especially high. No significant difference between the unit, proportional, modulus, and $|V(f)|^2$ weighting (see Table I in Ref. [31]) on the FFT and CNLS fit results is observed.

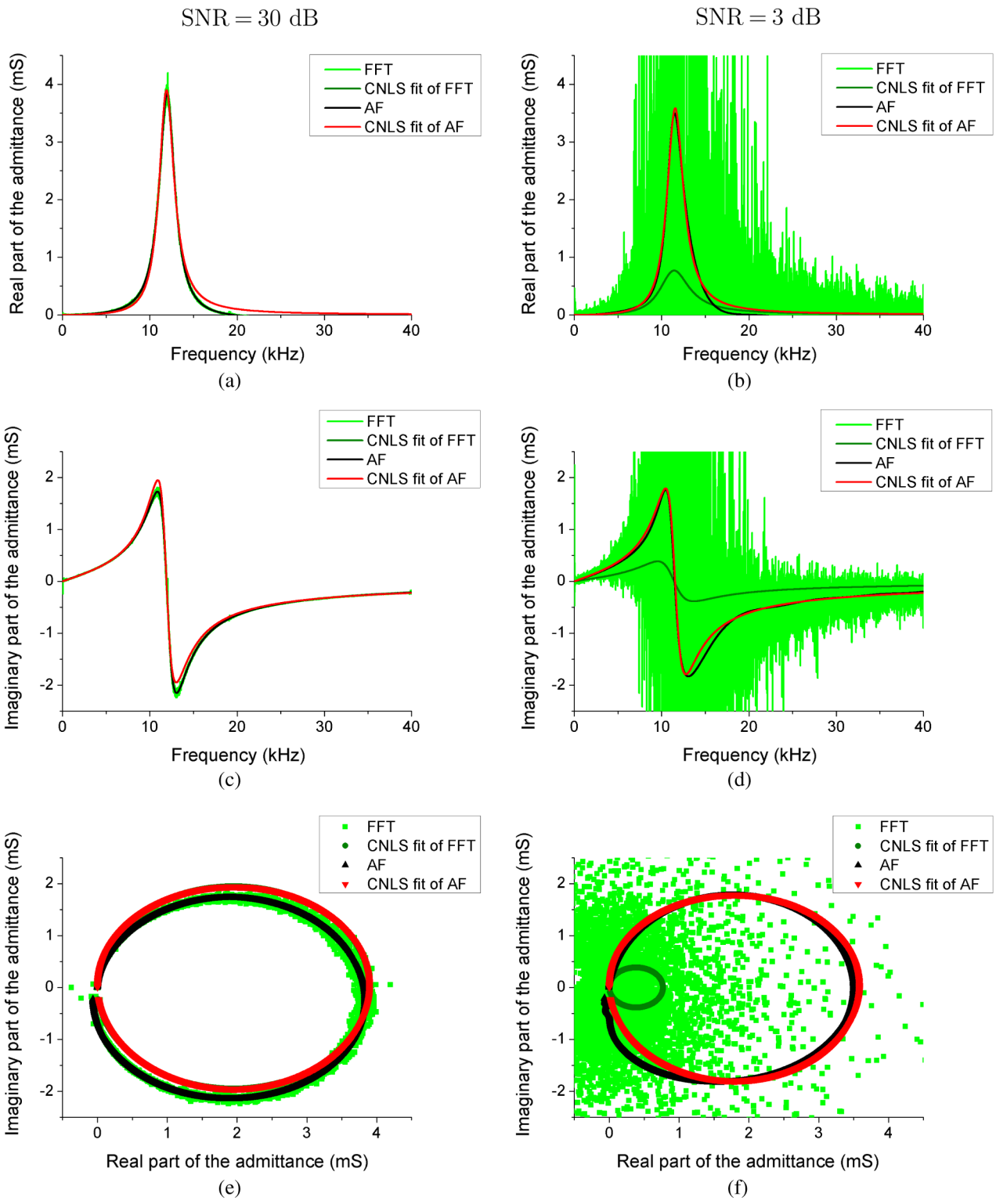

FIG. 3. Frequency dependences of admittance obtained with AF and FFT for the high and low experimentally studied SNRs. Panels (a), (c), and (e) correspond to SNR = 30 dB and show the admittance real and imaginary part spectra and the Nyquist plot, respectively. Panels (b), (d), and (f) correspond to SNR = 3 dB. Light green is used to show the raw admittance spectrum obtained by the FFT, and dark green is used to show the CNLS fit of the corresponding spectra. The admittance spectra obtained by AF are shown in black, and the CNLS fit of it is shown in red. The CNLS fits for AF and FFT in panels (a), (c), and (e) are overlapping.

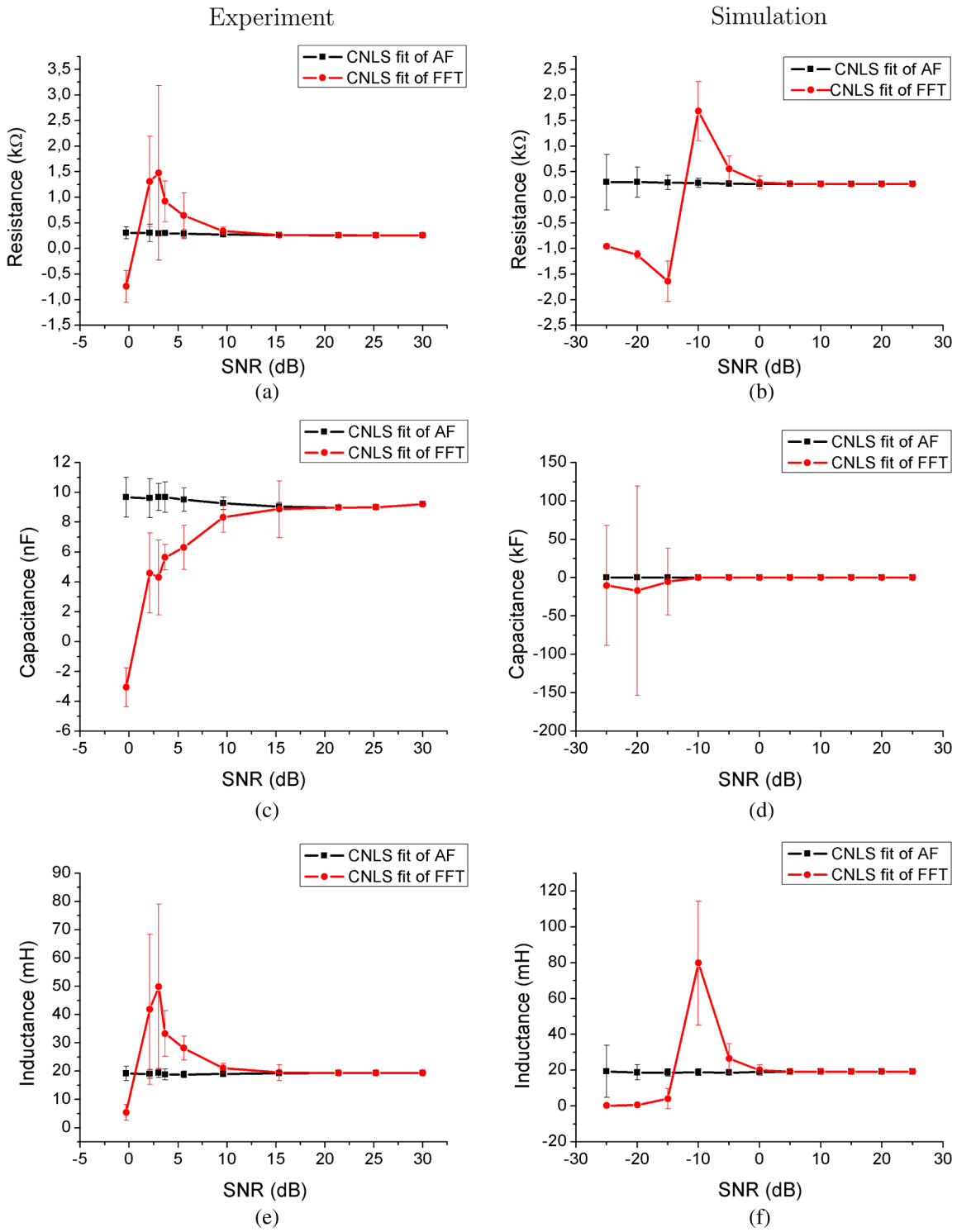

FIG. 4. Dependence of the obtained circuit elements ratings on the signal-to-noise ratio exhibiting the AF advances in noise immunity with respect to the FFT. Black squares are the results of the CNLS fit of the IS obtained by the FFT. Red circles denote the circuit element ratings obtained by AF. The statistics over four experiments for each SNR allow us to add the error bars (99.9% reliability). Panels (a), (c), and (e) are for the experimentally generated noise for resistance, capacitance, and inductance, respectively. Panels (b), (d), and (f) are for the digital artificial noise for resistance, capacitance, and inductance, respectively. AF gives correct results for all studied SNRs for both experimental noise and noise modeling. The FFT fails at 5 dB for experimental data and at 0 dB for noise modeling.

TABLE I. RLC-circuit parameter estimations with 99.9% confidence intervals for different methods and SNRs. The last columns list the rms between the CNLS fit of the FFT yield and that obtained with the AF spectrum with respect to the FFT.

SNR (dB)	Method	R (Ω)	C (nF)	L (mH)	Residual type	Residual rms (μS)
30	AF and CNLS	256.7 ± 0.4	9.209 ± 0.007	19.36 ± 0.02	AF vs FFT	30
	FFT and CNLS	256.7 ± 0.3	9.207 ± 0.006	19.360 ± 0.007	CNLS vs FFT	110
3	AF and CNLS	290 ± 50	9.7 ± 0.9	19 ± 2	AF vs FFT	3000
	FFT and CNLS	1000 ± 2000	4 ± 3	50 ± 30	CNLS vs FFT	2000
30	AF and AM	262.1 ± 0.4	9.37 ± 0.02	19.04 ± 0.04	⋯	
3		300 ± 60	9 ± 1	21 ± 3	⋯	

Contrary to the FFT, the IS obtained by the AF method does not degrade with decreasing SNR, and the R, L, and C ratings calculated from them stay intact. We relate this effect to the noise-canceling property of AF. Eliminating the uncorrelated with excitation voltage noise from the IS prevents its influence on the circuit parameters' estimation. Being the simplest artificial intelligence, AF automatically recognizes the useful signal in the time-domain data and separates it from the signal distorted by the background noise.

It is not surprising that the confidence intervals (CIs) of the circuit element ratings for both the AF and FFT methods increase with decreasing SNR. In the AF method, the CI grows with decreasing SNR slower than in the case of the FFT method. The lower spectrum AF vs FFT rms in the high-SNR case is also not surprising because, as can be seen from the FFT data in Fig. 3(e), the RLC-circuit IS is slightly distorted at high frequencies due to ADC nonideality. The AF semi-IIR model is more flexible than the RLC-circuit model, so the first one maintains this effect.

Interestingly, in the case of low SNR, the residual error between the IS obtained by the FFT method and the spectra obtained with the AF method is higher than that of the FFT spectra and their CNLS fit. So, the least-mean-squares criterion is not adequate for the low SNR and highly distorted IS. The present results ascertain this figure.

The smooth nature of the IS obtained by AF makes it possible to use simple algebraic methods to estimate the circuit element ratings, which gives a significant advantage in computation power and eliminates the human factor. For the RLC circuit, the element ratings can be expressed via the impedance magnitude minimum position frequency $f_{\min}$, the impedance magnitude minimum value $|Z(f_{\min})|$, and the frequency of the admittance imaginary part maximum position $f_{\max}$ as $R = |Z(f_{\min})|$, $L = Rf_{\max}/[2\pi(f_{\max}^2 - f_{\min}^2)]$, and $C = 1/[L(2\pi f_{\min})^2]$. The results of the AM fit are given in the last two rows of Table I for comparison with the results of the CNLS. The element rating CI obtained by the AM are not overlapped with the CI for high-SNR CNLS fits because the AM uses only a few points from the IS at middle frequencies, and the mentioned high-frequency systematic distortion (ADC nonideality) does not affect them.

V. PRACTICAL EXAMPLE: APPLICATION FOR BIOSENSORS

In this section, we present a practical example of biosensing in which AF gives a significant advantage with respect to the FFT. The investigated system is a multielectrode array MEA-200/30 (Multichannel Systems GmbH, Germany, 30-μm electrode diameter) covered by HeLa cells in phosphate-buffered saline (Biolot, Russia) *in vitro* under microscope

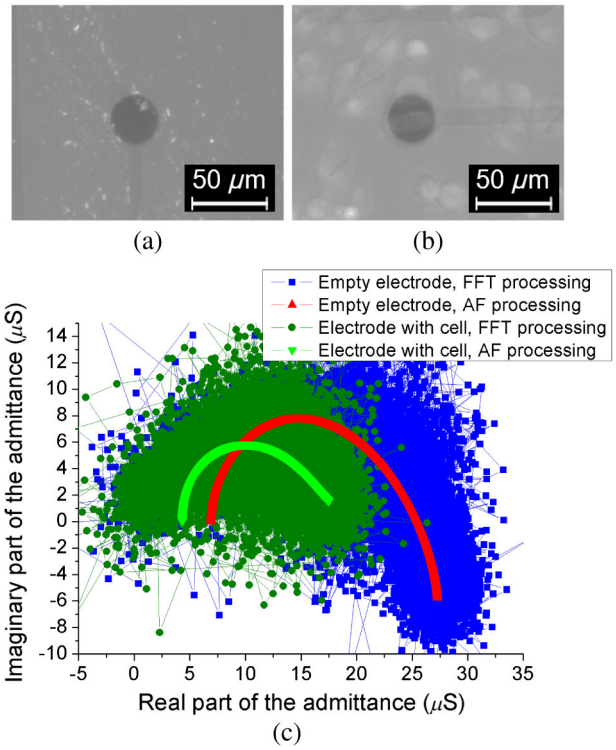

FIG. 5. Application AF for the biosensing EIS. (a) Photograph of the empty electrode. (b) Photograph of the electrode covered by the cell. The diameter of the electrodes is 30 μm. (c) Nyquist plot of the obtained IS. Red and light green denote the IS obtained by AF of the empty and the covered by cell electrodes, respectively. Blue and dark green denote the IS obtained by FFT of the empty and the covered by cell electrodes, respectively. One sees that the AF IS is more informative with respect to the FFT IS; for example, it can be seen acceptance of the Giaever-Keese model [20]. The acronyms used in figure are immittance spectrum (IS) and fast Fourier transformation (FFT).

study. The HeLa cells are obtained from the Bank of Cell Cultures of the Institute of Cytology of the Russian Academy of Sciences. The IS is measured between a large rectangle reference electrode ($50 \times 250\ \mu m^2$, not presented in photographs) and an empty electrode [Fig. 5(a)] and between a reference electrode and an electrode covered by a single cell [see Fig. 5(b)]. We use the described setup for the IS measurement. The feedback resistor rating is 1 MΩ, and all other parameters are same as the RLC-circuit study. The results are presented on Fig. 5(c).

One can see that the IS obtained by the FFT is distorted by interference from the microscope, and no useful information can be achieved from it. However, the IS obtained by the AF method is noise-free and more informative; for example, the bright green and red arcs' origins (their left ends) are displaced, as predicted by the Giaever-Keese model [20].

VI. CONCLUSION AND OUTLOOK

In this study, we develop the theory of AF IS processing and compare this approach with the FFT. The main outcome is that the processing of time-domain impedance data collected at low-SNR conditions with the FFT yields distorted and inadequate IS, but the IS obtained with the AF method is robust with respect to noises even at negative SNR. The developed AF-based software for IS data processing can be obtained from the authors.

The developed AF-based approach makes impedance and admittance spectroscopy much more sensitive and brings it to another level in all areas: material science, biophysics, electronic devices characterization, and quality control in the semiconductor industry. Moreover, the time-domain impedance data (V_k and J_k sequences), which cannot be interpreted with the FFT approach, can be analyzed with the AF-based one with a higher probability of success.

This technique can find practical use in studying dynamic and nonreversible systems under low-SNR conditions. It is especially important for biological systems because their investigation requires usage of low excitation voltage and low current response, which results in decreasing the signal-to-noise ratio. Portable biosensors based on the developed method will be robust to external interferences and noises. The moderate computation power and memory requirements also make AF appropriate to employ in this area.

ACKNOWLEDGMENTS

D. S. would like to thank Y. Well and H. Child for their multifaceted recommendations, without which this study would never have been started. We like to thank A. V. Nalitov, O. I. Utesov, I. N. Terterov, and A. L. Chernev for useful criticism and N. A. Knyazev for his help in describing the biological experiment.

APPENDIX A: FUNCTIONAL MINIMIZATION

One can see that Eq. (1) can be written in the terms of the Toeplitz matrices

$$L - \max(\ell_n, \ell_d) \left\{ \left\| \overbrace{\begin{matrix} V_{\ell_n} & \dots & V_2 & V_1 & V_0 \\ V_{\ell_n+1} & \dots & V_3 & V_2 & V_1 \\ \dots & & & & \\ V_{\ell_n+r} & \dots & V_{r+2} & V_{r+1} & V_r \\ \dots & & & & \\ \dots & & & & \\ \dots & & & & \\ \dots & & & & \end{matrix}}^{\hat{V}} \right| \overbrace{\begin{matrix} J_{\ell_d} & \dots & J_2 & J_1 & J_0 \\ J_{\ell_d+1} & \dots & J_3 & J_2 & J_1 \\ \dots & & & & \\ J_{\ell_d+r} & \dots & J_{r+2} & J_{r+1} & J_r \\ \dots & & & & \\ \dots & & & & \\ \dots & & & & \\ \dots & & & & \end{matrix}}^{\hat{J}} \right\| \cdot \overbrace{\left\| \begin{matrix} n_0 \\ n_1 \\ n_2 \\ \dots \\ n_{\ell_n} \\ d_1 \\ d_2 \\ d_3 \\ \dots \\ d_{\ell_d} \end{matrix} \right\|}^{\vec{w}} = \overbrace{\left\| \begin{matrix} J_{\ell_d+1} \\ J_{\ell_d+2} \\ J_{\ell_d+3} \\ \dots \\ J_{\ell_d+r} \\ \dots \\ \dots \end{matrix} \right\|}^{\vec{J}_d}, \tag{A1}$$

where $\hat{V}$ and $\hat{J}$ are the Toeplitz matrices generated by the V_k and J_k sequences, respectively, $\vec{w}$ is a vector obtained by n_j and d_j WC concatenation, and $\vec{J}_d$ is the desired current response. In matrix notation, Eq. (3) takes the form

$$(\| \hat{V} \quad \hat{J} \| \vec{w} - \vec{J}_d)^2 = \min. \tag{A2}$$

It is well known that the solution of Eq. (A2) can be reduced to solving the linear system

$$\left\| \begin{matrix} \hat{V}^T \\ \hat{J}^T \end{matrix} \right\| \| \hat{V} \quad \hat{J} \| \vec{w} = \left\| \begin{matrix} \hat{V}^T \\ \hat{J}^T \end{matrix} \right\| \vec{J}_d. \tag{A3}$$

Thus, the functional Eq. (3) minimization problem leads to the $(\ell_n + \ell_d + 1) \times (\ell_n + \ell_d + 1)$ linear system on vector $\vec{w}$ of WC from which the admittance can be directly obtained with Eq. (10). To prevent any misunderstanding related with the existence of various physical dimensions

in Eq. (A3), we suggest the following normalization. The impedance Z should be normalized to the feedback resistor R_0, and all voltage inputs for the ADC should be normalized to the ADC range (see Fig. 2). This procedure makes all elements of $\hat{V}$, $\hat{J}$, $\vec{w}$, and $\vec{J}_d$ dimensionless.

APPENDIX B: NOISE IMMUNITY OF AF

Now we use the normalization notation mentioned above and explain the noise-canceling property of AF in the identification mode. To do so, we introduce the Toeplitz matrix $\hat{\varepsilon}$ generated by the current noise ε_k sequence in the same manner as $\hat{J}$ is generated by J_k and add $\hat{\varepsilon}$ to $\hat{J}$. Thus, Eq. (3) transforms into

$$\left(\begin{Vmatrix} \hat{V}^T\hat{V} & \hat{V}^T\hat{J} \\ \hat{J}^T\hat{V} & \hat{J}^T\hat{J} \end{Vmatrix} + E_L\right)\vec{w}^* = \begin{Vmatrix} \hat{V}^T\vec{J}_d \\ \hat{J}^T\vec{J}_d \end{Vmatrix} + E_R, \tag{B1}$$

where

$$E_L = \begin{Vmatrix} 0 & \hat{V}^T\hat{\varepsilon} \\ \hat{\varepsilon}^T\hat{V} & \hat{\varepsilon}^T\hat{J} + \hat{J}^T\hat{\varepsilon} + \hat{\varepsilon}^T\hat{\varepsilon} \end{Vmatrix}, \tag{B2}$$

$$E_R = \begin{Vmatrix} \hat{V}^T\vec{\varepsilon} \\ \hat{\varepsilon}^T\vec{J}_d + \hat{J}^T\vec{\varepsilon} + \hat{\varepsilon}^T\vec{\varepsilon} \end{Vmatrix} \tag{B3}$$

are perturbations, $\vec{\varepsilon}_k = \varepsilon_k$, and $\vec{w}^*$ is the perturbed WC vector. If noise ε is uncorrelated with the EV and current, then all products in E_R and E_L with $\hat{V}$ and $\hat{J}$ are equal to zero, and perturbation depends only on the noise correlation function. Moreover, if the noise is autocorrelated, then $E_R = 0$, and E_L is a diagonal matrix with ℓ_d nonzero elements. The L_2 norm of E_L in this case is the noise mean-square value $\langle\varepsilon^2\rangle$. In the basis of the standard approach for the linear system error estimation [42–44], one can write

$$\frac{|\vec{w} - \vec{w}^*|}{|\vec{w}|} \le \frac{\langle\varepsilon^2\rangle\nu}{A}, \tag{B4}$$

where ν and A are the condition number and L_2 norm of the main matrix in Eq. (A3), respectively. The fact that $\langle\varepsilon^2\rangle$ is independent of the filtering order allows one to obtain the following estimation for the root-mean-square of the relative error ($\mathrm{rms}_{\mathrm{error}}$) in WC from Eq. (B4):

$$\mathrm{rms}_{\mathrm{error}} = \frac{1}{|\vec{w}|}\sqrt{\frac{\sum_{j=0}^{\ell_n+\ell_d}(\vec{w}_j - \vec{w}_j^*)^2}{\ell_n + \ell_d + 1}} \le \frac{\langle\varepsilon^2\rangle\nu}{A\sqrt{\ell_n + \ell_d + 1}}. \tag{B5}$$

In the most favorable case, $\nu = 1$ and the $\mathrm{rms}_{\mathrm{error}}$ of the WC falls off as $1/\sqrt{\ell_n + \ell_d + 1}$, which is reminiscent of the classical statistics law for the signal-averaging technique. If the FIR model is used, there is no influence of noise on the WC (compare with Ex. 6 on p. 226 in Ref. [34]).

It should be noticed that the linear dependence of the columns in $\| \hat{V}\ \hat{J} \|$ leads to the increasing of ν, and, as a corollary, to the instability of the system (A3). Such linear dependence can arise in the case of a short periodic EV or in the case of pure resistance-type impedance. In this case, for better robustness, the singular value decomposition can be used directly to solve Eq. (A1) [45].

APPENDIX C: ON THE SWEEP-SHAPE EXCITATION VOLTAGE

The Fourier image of the linear-sweep-shape signal is numerically investigated in Ref. [28] [see Fig. 4(e)] and analytically obtained in the general form in Ref. [46]. By setting $r(t)$ in Eq. (9) in Ref. [46] to a rectangular function with the sweep-time interval width, and by applying Eqs. (8.250.2) and (8.250.3) from Ref. [47], we obtain the difference between the Frensel integrals, which is close to the rectangular function with the $\pm f_B$ interval width.

[1] Evgenij Barsoukov and J. Ross Macdonald, *Impedance Spectroscopy: Theory Experiment and Applications*, 2nd ed. (Wiley-Interscience, New York, 2005).

[2] Vadim F. Lvovich, *Impedance Spectroscopy: Applications to Electrochemical and Dielectric Phenomena*, 1st ed. (Wiley, New York, 2012).

[3] A. A. Lebedev, Jr., A. A. Lebedev, and D. V. Davydov, Capacitance measurements for diodes in the case of strong dependence of the diode-base series resistance on the applied voltage, Semiconductors **34**, 115 (2000).

[4] N. A. Poklonski, N. I. Gorbachuk, S. V. Shpakovski, and A. Wieck, Equivalent circuit of silicon diodes subjected to high-fluence electron irradiation, Tech. Phys. **55**, 1463 (2010).

[5] K. J. Russell, F. Capasso, V. Narayanamurti, H. Lu, J. M. O. Zide, and A. C. Gossard, Scattering-assisted tunneling: Energy dependence, magnetic field dependence, and use as an external probe of two-dimensional transport, Phys. Rev. B **82**, 115322 (2010).

[6] L. S. Berman and A. A. Lebedev, *Capacitance Spectroscopy of Deep Levels* (in Russian) (Nauka, Moscow, 1981).

[7] Lucjan Jacak, Arkadiusz Wojs, and Pawe Hawrylak, *Quantum Dots*, 1st ed., NanoScience and Technology (Springer-Verlag Berlin, Verlag, 1998), Chap. 7, pp. 83–96.

[8] Yuanhua Lin, Lei Jiang, Rongjuan Zhao, and Ce-Wen Nan, High-permittivity core/shell structured NiO-based ceramics and their dielectric response mechanism, Phys. Rev. B **72**, 014103 (2005).

[9] K. Arbi, M. Tabellout, M. G. Lazarraga, J. M. Rojo, and J. Sanz, Non-Arrhenius conductivity in the fast lithium conductor $Li_{1.2}Ti_{1.8}Al_{0.2}(PO_4)3$: A ^{7}Li NMR and electric impedance study, Phys. Rev. B **72**, 094302 (2005).

[10] Luca Mesin and Marco Scalerandi, Effects of transducer size on impedance spectroscopy measurements, Phys. Rev. E **85**, 051505 (2012).
[11] Debanjan Das, Kumar Shiladitya, Karabi Biswas, Pranab Kumar Dutta, Aditya Parekh, Mahitosh Mandal, and Soumen Das, Wavelet-based multiscale analysis of bioimpedance data measured by electric cell-substrate impedance sensing for classification of cancerous and normal cells, Phys. Rev. E **92**, 062702 (2015).
[12] Giovanni Barbero and I. Lelidis, Evidence of the ambipolar diffusion in the impedance spectroscopy of an electrolytic cell, Phys. Rev. E **76**, 051501 (2007).
[13] I. Lelidis and Giovanni Barbero, Effect of different anionic and cationic mobilities on the impedance spectroscopy measurements, Phys. Lett. A **343**, 440 (2005).
[14] Jean-Baptiste Jorcin, Mark E. Orazem, Nadine Pébère, and Bernard Tribollet, CPE analysis by local electrochemical impedance spectroscopy, Electrochim. Acta **51**, 1473 (2006).
[15] Shuoqin Wang, Mark Verbrugge, Luan Vu, Daniel Baker, and John S. Wang, Battery state estimator based on a finite impulse response filter, J. Electrochem. Soc. **160**, A1962 (2013).
[16] Ying Ting Set, Erik Birgersson, and Joachim Luther, Predictive Mechanistic Model for the Electrical Impedance and Intensity-Modulated Photocurrent and Photovoltage Spectroscopic Responses of an Organic Bulk Heterojunction Solar Cell, Phys. Rev. Applied **5**, 054002 (2016).
[17] Jianjun Tian, Ting Shen, Xiaoguang Liu, Chengbin Fei, Lili Lv, and Guozhong Cao, Enhanced performance of PbS-quantum-dot-sensitized solar cells via optimizing precursor solution and electrolytes, Sci. Rep. **6**, 23094 (2016).
[18] Uwe Rau, Daniel Abou-Ras, and Thomas Kirchartz, *Advanced Characterization Techniques for Thin Film Solar Cells*, 1st ed. (Wiley-VCH, New York, 2011), Chap. 4, pp. 81–105.
[19] Ivar Giaever and Charles R. Keese, A morphological biosensor for mammalian cells, Nature (London) **366**, 591 (1993).
[20] Joachim Wegener, Charles R. Keese, and Ivar Giaever, Electric cell–substrate impedance sensing (ECIS) as a noninvasive means to monitor the kinetics of cell spreading to artificial surfaces, Exp. Cell Res. **259**, 158 (2000).
[21] Sverre Grimnes and Orjan G. Martinsen, *Bioimpedance and Bioelectricity Basics*, 3rd ed. (Academic Press, New York, 2015).
[22] Jonathan Rivnay, Pierre Leleux, Adel Hama, Marc Ramuz, Miriam Huerta, George G. Malliaras, and Roisin M. Owens, Using white noise to gate organic transistors for dynamic monitoring of cultured cell layers, Sci. Rep. **5**, 11613 (2015).
[23] M. Weckström, E. Kouvalainen, and M. Juusola, Measurement of cell impedance in frequency domain using discontinuous current clamp and white-noise-modulated current injection, Pfluegers Arch. **421**, 469 (1992).
[24] Seon-Ah Jin, Shishir Poudyal, Ernesto E. Marinero, Richard J. Kuhn, and Lia A. Stanciu, Impedimetric dengue biosensor based on functionalized graphene oxide wrapped silica particles, Electrochim. Acta **194**, 422 (2016).
[25] E. Oran Brigham, *The Fast Fourier Transform: An Introduction to Its Theory and Application* (Prentice-Hall, Englewood Cliffs, NJ, 1973).
[26] Lawrence R. Rabiner and Bernard Gold, *Theory and Application of Digital Signal Processing* (Prentice-Hall, Englewood Cliffs, NJ, 1975).
[27] Byoung-Yong Chang and Su-Moon Park, Electrochemical impedance spectroscopy, Annu. Rev. Anal. Chem. **3**, 207 (2010).
[28] G. S. Popkirov and R. N. Schindler, A new impedance spectrometer for the investigation of electrochemical systems, Rev. Sci. Instrum. **63**, 5366 (1992).
[29] Malte Leisner, Jürgen Carstensen, and Helmut Föll, FFT impedance spectroscopy analysis of the growth of anodic oxides on (100) P-Si for various solvents, J. Electroanal. Chem. **615**, 124 (2008).
[30] J. Ross Macdonald and J. A. Garber, Analysis of impedance and admittance data for solids and liquids, J. Electrochem. Soc. **124**, 1022 (1977).
[31] James Ross Macdonald, Comparison and application of two methods for the least squares analysis of immittance data, Solid State Ionics **58**, 97 (1992).
[32] Franz Hamilton, Tyrus Berry, and Timothy Sauer, Ensemble Kalman Filtering without a Model, Phys. Rev. X **6**, 011021 (2016).
[33] Dirk Schütte, S. Z. Sayed Hassen, Kai S. Karvinen, Toby K. Boyson, Abhijit G. Kallapur, Hongbin Song, Ian R. Petersen, Elanor H. Huntington, and Michèle Heurs, Experimental Demonstration of Frequency Autolocking an Optical Cavity Using a Time-Varying Kalman Filter, Phys. Rev. Applied **5**, 014005 (2016).
[34] Bernard Widrow and Peter N. Stearns, *Adaptive Signal Processing*, Prentice-Hall Signal Processing Series (Prentice-Hall, Englewood Cliffs, NJ, 1985).
[35] W. Denda, *Noise as Source of Information* (in Russian) (Mir, Moscow, 1993), Chap. 6, pp. 135–150.
[36] W. Denda, *Rauschen als Information* (in German) (Technik, Berlin, 1988).
[37] E. C. Levy, Complex-curve fitting, IRE transactions on automatic control **1**, 37 (1959).
[38] Digby D. Macdonald, A method for estimating impedance parameters for electrochemical systems that exhibit pseudoinductance, J. Electrochem. Soc. **125**, 2062 (1978).
[39] Y.-T. Tsai and D. H. Whitmore, Nonlinear least-squares analyses of complex impedance and admittance data for solid electrolytes, Solid State Ionics **7**, 129 (1982).
[40] Gregory M. Dittami, H. Edward Ayliffe, Curtis S. King, and Richard D. Rabbitt, A multilayer MEMS platform for single-cell electric impedance spectroscopy and electrochemical analysis, J. Microelectromech. Syst. **17**, 850 (2008).
[41] Jeffrey C. Lagarias, James A. Reeds, Margaret H. Wright, and Paul E. Wright, Convergence properties of the Nelder-Mead simplex method in low dimensions, SIAM J. Optim. **9**, 112 (1998).
[42] V. M. Verzbitskii, *Computation Linear Algebra* (in Russian) (Visshay Shkola, Moscow, 2007), Chap. 8.3, pp. 307–313.
[43] John R. Rice, *Matrix Computations and Mathematical Software*, McGraw-Hill Computer Science Series (McGraw-Hill, New York, 1981), Chap. 9.B, pp. 112–115.

[44] H. Golub and Charles F. Van Loan, *Matrix Computations*, 3rd ed., Johns Hopkins Studies in the Mathematical Sciences (Johns Hopkins University Press, London, 1996), Chap. 2.7.2, pp. 80–82, Eq. 2.7.4.

[45] Charles L. Lawson and Richard J. Hanson, *Solving Least Squares Problems*, Classics in Applied Mathematics Vol. 15 (Society for Industrial and Applied Mathematics, Philadelphia, 1987), Chap. 18, pp. 107–120.

[46] Maurice Rozenberg, Linear sweep synthesis, Computer Music Journal **6**, 65 (1982).

[47] I. S. Gradshteyn and M. Ryzhik, *Table of Integrals, Series, and Products*, 6th ed. (Academic Press, New York, 2000) p. 880.